Electrochemical Impedance Spectroscopy Study of Porous Anodic Alumina Films Fabricated at Low Temperature

Di MA [1]*, Shuying LI [2], Xinyu LYU [4], Shubai LI [3], Yang CAO [1]

[1] *School of Chemistry & Environmental Engineering, Jiangsu University of Technology, Changzhou, China*
[2] *Department of Chemical Engineering, Dalian University of Technology, Dalian, China*
[3] *Department of Chemical Engineering, Changzhou Institute of Engineering Technology, Changzhou, China*
[4] *Jiangsu Key Laboratory of Advanced Catalytic Materials and Technology, Changzhou University, Changzhou, China*

crossref http://dx.doi.org/10.5755/j02.ms.30047

Received 29 October 2021; accepted 01 June 2022

A method of fabrication of AAO film in 0.3 mol/L $H_2C_2O_4$ by adding 1,2-propanediol(PROH) and at sub-zero temperature has been proposed. The electrochemical characteristics of the barrier and porous layers of AAO films before and after pore-filling are examined using electrochemical impedance spectroscopy (EIS). It is shown that the high and medium frequency range corresponds to the barrier layer properties and the low frequency ranges reflect the sealed porous layer properties. The calculated thickness of the barrier layer is in the range of 1 ~ 18 nm. The resistance (R_b) and the thickness (δ_b) of the barrier layer increase and the capacitance of the barrier layer (CPE_b) decrease with the volume percentage of PROH increasing from in electrolyte from 25 % to 75 %. The surface non-homogeneity of AAO film goes better by pore-filling, leading to a decrease in the capacitance of the porous layer (CPE_p) and an increase in the porous layer thickness.

Keywords: anodic aluminum oxide film, low temperature anodization, pore-filling, electrochemical impedance spectroscopy.

1. INTRODUCTION

Electrochemical impedance spectroscopy (EIS) has been widely used in physics, biology, and electrochemistry. It has been used to evaluate dissolution and passivation phenomena [1, 2], study organic coatings [3, 4] and electrodeposition properties [5, 6], determine battery parameters [7, 8], and study electrical properties of solid electrolyte [9, 10]. As an effective detection method, EIS is often used to study the properties of the porous Anodic Aluminium Oxide (AAO) films under different conditions to make up for the lack of TEM and SEM in determining the microstructure parameters of AAO films.

Fig. 1 shows the schematic diagram of the AAO film, which has a double-layer structure, with a thin dense barrier layer on the bottom layer and a thick porous layer on top. Before filling, the Equivalent Circuit is mainly composed of the barrier capacitor [11], because the electrolyte in the pores has a higher conductivity, which leads to a smaller resistance R_p of the porous layer. Regarding the AAO film as an ideal capacitor or dielectric, the barrier thickness (δ_b) can be determined [12]. During the pore-filling experiment, the electrolyte is neutral and will not dissolve the AAO film, which leads to new oxides being formed in the porous layer. Therefore, the electrochemical impedance value of the porous layer increases after the pore is filled (Fig. 1 b), and the thickness (δ_p) of the pore-filled part of the porous layer can be determined. At present, the AAO films can be used as a template for preparing various nanomaterials such as nanoparticles, nanowires and nanotubes.

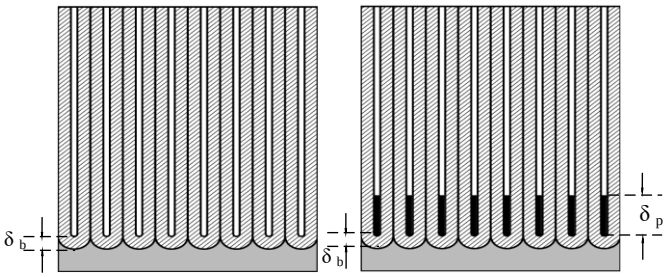

Fig. 1. A schematic picture of AAO films (a) before and (b) after pore-filling

The main factors in determining the structural parameters of AAO films and the mechanism of porous structure formation have been well studied, AAO as a template for nanofabrication has not been completely understood. The main question at present is how to achieve the minimum pore size of AAO films with a neat array of holes. In this paper, to achieve low temperature oxidation, 1, 2-propanediol is added to the electrolyte to achieve an oxidation temperature of sub-zero temperature. The Electrochemical Impedance Spectroscopy (EIS) technique was used to characterize the changes in the thickness of the barrier layer and porous layer of AAO films prepared in oxalic acid with low oxidation temperatures and electrolyte compositions under low temperature conditions. EIS technology was used to characterize the characteristics of the barrier layer and the porous layer by filling technology.

2. EXPERIMENTAL

The thickness of the aluminum foil is 0.25 mm, and the purity is 99.99 %. First, the pre-treated aluminum foils

*Corresponding author. Tel.: +86-15951207428.
E-mail address: *madi@jsut.edu.cn* (D. Ma)

were prepared. The anodization was performed in a mixture solution of 1, 2-propanediol and or 0.3 mol/L $H_2C_2O_4$ at sub-zero temperature (0 ～-10 °C) for 1 h at a constant 60 V using a DC power supply. The aluminum foil was used as the anode and the platinum sheet as the cathode.

After the AAO films were thoroughly cleaned in deionized water, a pore-filling experiment was carried out at a current density of 0.5 mA/cm^2. The experimental equipment is Princeton EG&G173 potentiostat. The experiment uses a three-electrode system, the reference electrode is a saturated calomel electrode (SCE), and the auxiliary electrode is a platinum electrode. The EIS test was carried out in a mixed solution composed of 0.5 mol/L H_3BO_3 and 0.05 mol/L $Na_2B_4O_7$ at 20 °C and the filling time is 10 minutes. Princeton EG&G273 potentiostat and Powersuit software were used for measurement. The electrochemical impedance perturbation voltage is 10 mV, the frequency range is 10^{-1} ~ 10^5 Hz, and the frequency is scanned from high frequency to low frequency. The impedance spectra were further analyzed using ZsimpWin software. The EIS spectrogram adopts ZSimpWin software, selects the appropriate equivalent circuit to analyze and solve the various parameters.

3. RESULTS AND DISCUSSION

Fig. 2 shows the Bode diagrams of the AAO films prepared in 0.3 mol/L $H_2C_2O_4$ solutions with different temperatures and 1,2-propanediol(PROH) contents before and after filling the holes. The changes in impedance with the frequency are shown by the above curves in the figure.

When the volume percentage of PROH is 25 %, the Bode diagram (Fig. 2 a) before the hole filling experiment shows that there is a phase angle peak and a horizontal impedance value in the frequency of 10^3 Hz. It shows that the system has only one relaxation time, and there is only one rate-controlling step in the electrochemical process, which is the time constant caused by the charge transfer on the interface between the electric double layer and the barrier layer and the bottom of the hole ($\tau_b=R_bC_b$). Since the electrolyte in the pores can contact the layer, the high conductivity of the electrolyte makes the impedance R_P of the porous layer too small compared to R_b, so the horizontal impedance and phase angle peaks of the corresponding porous layer are not shown in Fig. 2.

The Bode diagram after the hole filling (Fig. 2 b) shows that there are two phase angle peaks in the frequency of 1 Hz and 1×10^4Hz, indicating that the system has two relaxation times, which is close to the frequency position of the phase angle peak barrier layer of the AAO film before pore-filling. The other phase angle peak is at 1 Hz, which is the time constant ($\tau_P=R_PC_P$) caused by the charge transfer on the interface between the pore and the electrolyte.

Several studies [13 – 16] indicate that the middle and high frequency bands on the spectrum reflect the characteristics of the closed barrier layer, while the low frequency band reflects the characteristics of the closed part of the porous layer. The secondary oxidation process is the process of filling the holes of the AAO film in the neutral electrolyte. When the porous layer is filled with holes, it will be reflected on the Bode curve. When the volume percentage of PROH is 50 %, the curve shape of the bode diagram (Fig. 2 c and d) before and after the hole filling is basically the same as that of the 25 % PROH, that is, there is only one barrier layer before the hole filling.

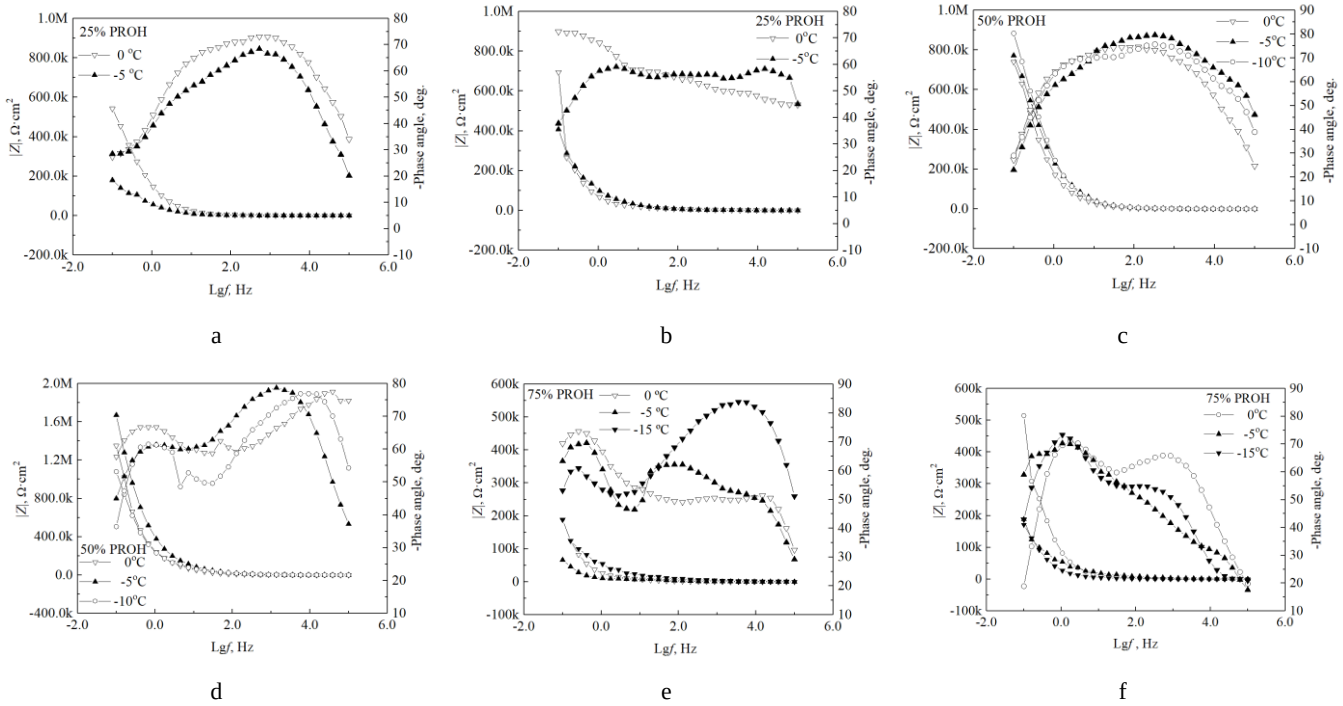

Fig. 2. Bode plots of AAO films formed in 0.3 mol/L $H_2C_2O_4$ with various concentrations of PROH at different temperatures: a, c, e – before pore-filling; b, d, f – after pore-filling

The phase angle peak, after the hole filling, there are two phase angle peaks that respectively reflect the barrier layer and the porous layer. However, when the volume percentage of PROH is 75 %, there are two phase angle peaks in the AAO film's bode diagram (Fig. 2 e), and these two phase angle peaks are more obvious after the hole filling (Fig. 2 d).

The above situation can be explained by the changes in the pore size and porosity of the AAO films caused by the changes in the temperature of the electrolyte and the content of PROH. As the content of PROH increases and the temperature decreases, the pore size and porosity of the films decrease. Therefore, the phase angle peak of the porous layer before the pore-filling is reflected on the bode plots, but it is not very obvious, and it is fully reflected after the pore-filling.

Based on the above discussion, the equivalent circuit of the AAO film before and after the pore-filling experiment is represented by the models shown in Fig. 3a and b, respectively. The impedance value (Z) is expressed by Eq. 1 and Eq. 2:

$$Z(\omega) = R_{el} + \frac{R_b}{1+(j\omega R_b CPE_b)^{n_b}}; \quad (1)$$

$$Z(\omega) = R_{el} + \frac{R_p}{1+(j\omega R_p CPE_p)^{n_p}} + \frac{R_b}{1+(j\omega R_b CPE_b)^{n_b}}, \quad (2)$$

where Z is the impedance of the system; R_{el} is the solution resistance; C_P, R_P are the capacitance and resistance of the enclosed part of the porous layer; C_b, R_b are the capacitance and resistance of the barrier layer; ω is the angular frequency of the input sine wave, $\omega=2\pi f$; j is the imaginary part of the complex number, $j = (-1)^{1/2}$.

Fig. 4 shows a composite plan view of the fitting results of the equivalent circuit and the experimental data. There is a good fit between the experimental data and the theoretical value in the frequency range of $10^{-1} \sim 10^5$ Hz.

The impedance data can also be used to quantitatively analyze the film structure parameters. When the barrier layer is regarded as a plate capacitor, the thickness of the barrier layer can be calculated. The barrier layer capacitance and barrier layer thickness can be related as follows:

$$C_b = \varepsilon\varepsilon_0 S / \delta_b, \quad (3)$$

where $\varepsilon_0 = 8.854 \times 10^{-14}$ F/cm, which is the vacuum dielectric constant; $\varepsilon = 10$ is the relative constant of alumina $S = 1$ cm^2, which is the surface area of the electrode; δ_b is the thickness of the barrier layer. The filling part of the porous layer can be regarded as a barrier layer, so the thickness of the barrier layer and the porous layer can be obtained from CPE_b and CPE_p.

The electrochemical impedance parameters of AAO films are listed in Table 1. The film thickness is calculated according to Eq. 3. The fitting data of the EIS from Table 1 reveals that the magnitude of R_b and R_p, and the magnitude of CPE_b and CPE_p are basically the same before and after the pore-filling under different temperatures. Most of the n_b and n_p are greater than 0.8 and close to 1, indicating that CPE_b is close to the ideal capacitance C_b. In the fitting result, when the value of n is less than 0.8, when the experimental curve deviates too much from the fitting curve, the value of n will be too small, and the barrier layer thickness calculated by Eq. 3 is not accurate, so it is not listed in the table.

It can be seen from the table that the thickness of the barrier layer is 1 ~ 16 nm, which is basically consistent with the thickness of the barrier layer measured in the literature [17]. Previous studies [18] have shown that the thickness of the barrier layer is proportional to the oxidation voltage of the AAO film, as shown in the following formula:

$$\delta_b = aU_a, \quad (4)$$

where δ_b is the thickness of the barrier layer; a is the oxidation ratio of the barrier layer; U_a is the oxidation voltage. Under constant voltage, the oxidation ratio a will change with the change of electrolyte temperature and concentration [19]. For example, when the temperature is -5°C, when the PROH content in the 0.3 mol/L $H_2C_2O_4$ increases from 25 % to 75 %, the barrier layer thickness increases from 2.66 nm to 12.37 nm before the pore-filling, and the oxidation ratio increases from 0.044 nm/V increased to 0.206 nm/V after the pore-filling, the thickness of the barrier layer increased from 2.16 nm to 15.39 nm, and the oxidation ratio increased from 0.036 nm/V to 0.142 nm/V.

Table 1 also lists the thickness of the porous layer calculated according to Eq. 4 after filling the pores. As shown in the Table 1, the thickness of the porous layer is about 20 times the thickness of the corresponding barrier layer, in the range of 40 ~ 80 nm.

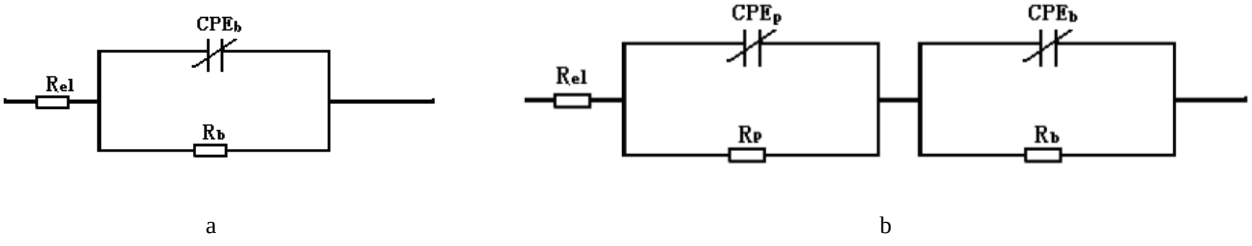

a b

Fig. 3. Equivalent circuit for the analysis of impedance spectra: a – before pore-filling; b – after pore-filling

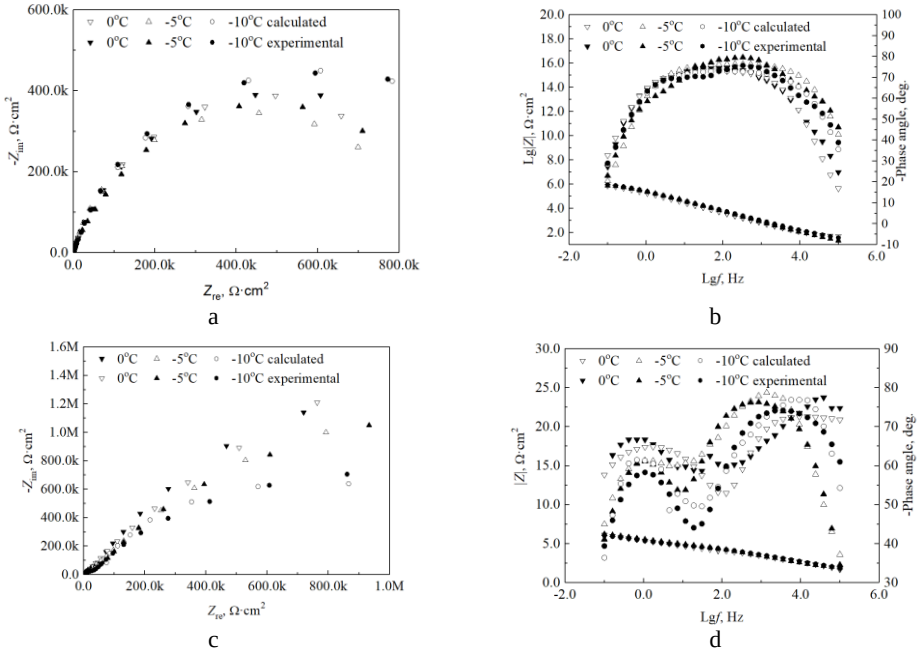

Fig. 4. Nyquist and Bode diagrams showing the fitting of the data to the equivalent circuit: a, b – before pore-filling; c, d – after pore-filling

Table 1. Electrochemical impedance parameters of AAO films formed in 0.3 mol/L $H_2C_2O_4$ before and after pore-filling

	PROH, %	*T*, °C	R_e, Ω·cm²	CPE_b, μF/cm²	δ_b, nm	n_b	$R_b \times 10^5$ Ω·cm²	CPE_p, μF/cm²	n_p	$R_p \times 10^5$ Ω·cm²	δ_p, nm
After pore-filling	25	-5	38.92	4.11	2.16	0.86	24.32	–	–	–	–
		0	22.36	7.89	1.12	0.88	24.35	–	–	–	–
	50	-10	49.03	–	–	–	–	0.10	0.80	7.19	86.8
		-5	44.13	2.98	2.97	0.86	0.13	0.20	0.98	6.80	43.62
		0	12.05	2.63	3.37	0.89	16.38	-	-	-	-
	75	-15	21.08	0.91	9.76	0.80	20.39	0.19	0.88	0.30	46.85
		-5	60.32	0.58	15.39	0.82	3.26	0.02	0.92	0.48	368.92
Before pore-filling	25	-5	17.91	3.33	2.66	0.81	1.89	–	–	–	
		0	433.1	3.39	2.60	0.82	8.04	–	–	–	
	50	-10	76.27	1.36	6.53	0.80	2.40	–	–	–	
		-5	18.65	1.62	5.46	0.87	2.73	–	–	–	
		0	46.07	1.84	4.82	0.97	4.60	–	–	–	
	75	-15	23.93	0.82	10.86	0.82	1.21				
		-5	13.05	0.72	12.37	0.85	8.73	–	–	–	
		0	43.31	0.64	13.79	0.82	10.49	–	–	–	

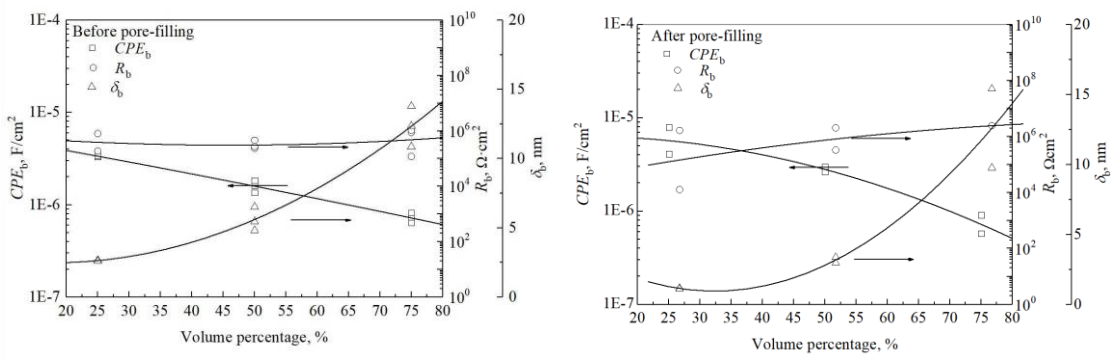

Fig. 5. Variation of electrochemical impedance parameters of AAO film formed in 0.3 mol/L $H_2C_2O_4$ with a different volume percentage of PROH before and after pore-filling

Fig. 5 shows the variation of the barrier layer capacitance CPE_b, barrier layer resistance R_b, and barrier layer thickness δ_b with the PROH content before and after the pore is filled. It can be seen from the figure that with the increase of PROH content before filling the pore, the capacitance of the barrier layer is obviously reduced while the resistance of the barrier layer increases slightly, and the thickness of the barrier layer increases accordingly (Fig. 5 a). The changing trend of the impedance parameters of the AAO film after the pore-filling is similar to that before the pore filling: with the increase of the PROH, the barrier layer capacitance decreases, the barrier layer resistance increases, and the barrier layer thickness also increases.

It can be seen from Fig. 5 that as the content of PROH increases, the capacitance of the barrier layer decreases, the resistance increases, and the ability of the barrier layer to resist electrolyte penetration increases, indicating that the thickness of the barrier layer increases with the increase of PROH content. In Table 1, under certain conditions of PROH content and oxidation temperature, the thickness of the barrier layer after sealing is slightly higher than that before sealing. This is because the defects in the barrier layer are filled after sealing, which reduces the capacitance of the barrier layer, thereby increasing the thickness of the barrier layer after sealing. The barrier layer is not a dense structure, and there are defects such as cracks and pits in the barrier layer. In a neutral electrolyte composed of 0.5 mol/L H_3BO_3 and 0.05mol L $Na_2B_4O_7$, BO_3^{3-} and $B_4O_7^{2-}$ migrate into the AAO films, and then stagnate in the film, and no longer migrate [20], so the new process of filling the hole the formation of oxide is firstly due to the migration of Al^{3+} ions and O^{2-} ions to fill the micropores in the barrier layer. After the microspores in the barrier layer are filled, new oxides begin to form in the pores of the porous layer.

The EIS results of the AAO film before and after the pore-filling show that there is only one phase angle peak reflecting the barrier layer before the pore-filling; two phase angle peaks appear after the pore -filling, and the middle and high frequency bands show closed blocking Layer characteristics, and the low frequency band reflects the characteristics of the closed part of the porous layer. Analyzing barrier layer capacitance CPE_b and barrier layer resistance R_b according to the established equivalent circuit model, it was calculated the barrier layer thickness that ranges from 1 to 18 nm.

4. CONCLUSIONS

This study uses alternating current impedance (EIS) technology to characterize the barrier layer and porous layer thickness changes of AAO films prepared in oxalic acid solutions with different oxidation temperatures and electrolyte components under low temperature conditions. The analysis of electrochemical parameters shows that with the increase of PROH content, the barrier layer capacitance CPE_b before and after the pore-filling decreases, the resistance R_b increases, and the barrier layer thickness δ_b increases. The pore-filling process improves the unevenness of the surface of the AAO film, the capacitance CPE_p of the porous layer decreases, and the corresponding porous layer thickness δ_p increases.

Acknowledgments

This work was sponsored by Changzhou Science and Technology Support Project (Social Development) (CE20215036), the Natural Science Foundation of the Jiangsu Higher Education Institutions (No.17KJA610002), Jiangsu Key Research and Social Development Project (No. BE2017649), Jiangsu Overseas Research & Training Program for University Prominent Young & Middle-aged Teachers and Presidents; Changzhou Institute of technology innovation team project (2020).

REFERENCES

1. **Farelas, F., Galicia, M., Brown, B., Nesic S.** Evolution of Dissolution Processes at the Interface of Carbon Steel Corroding in a CO_2 Environment Studied by EIS *Corrosion Science* 52 (2) 2010: pp. 509 – 517. http://dx.doi.org/10.1016/j.corsci.2009.10.007
2. **Gassa, L.M., Barbosa, M.R., Real, S.G., Vilche, J.R.**. The Application of EIS and XPS to Investigate the Dissolution and Passivation of Fe-Co Base Amorphous Alloys in $KHCO_3$-K_2CO_3 Buffers *Corrosion Science* 37 (7) 1995: pp. 1115 – 1129. http://dx.doi.org/10.1016/0010-938X(95)00018-F
3. **Margarit-Mattos, I.C.P.** EIS and Organic Coatings Performance: Revisiting Some Key Points *Electrochimica Acta* 354 2020: pp. 136725. http://dx.doi.org/10.1016/j.electacta.2020.136725
4. **Da Silva, T.C., Mallarino, S., Touzain, S., Margarit-Mattos I.C.P.** DMA, EIS and Thermal Fatigue of Organic Coatings *Electrochimica Acta* 318 2019: pp. 989 – 999. http://dx.doi.org/10.1016/j.electacta.2019.06.066
5. **Hasannejad, H., Shahrabi, T., Jafarian, M., Rouhaghdam A.S.** EIS Study of Nano Crystalline Ni-Cerium Oxide Coating Electrodeposition Mechanism *Journal of Alloys and Compounds* 509 (5) 2011: pp. 1924 – 1930. http://dx.doi.org/10.1016/j.jallcom.2010.10.089
6. **Huerta Garrido, M.E., Pritzker, M.D.** EIS and Statistical Analysis of Copper Electrodeposition Accounting for Multi-Component Transport and Reactions *Journal of Electroanalytical Chemistry* 594 (2) 2006: pp. 118 – 132. https://doi.org/10.1016/j.jelechem.2006.05.026
7. **Babaeiyazdi, I., Rezaei-Zare, A., Shokrzadeh, S.** State of Charge Prediction of EV Li-ion Batteries Using EIS: A Machine Learning Approach *Energy* 223 2021: pp. 120116. http://dx.doi.org/10.1016/j.energy.2021.120116
8. **Cruz-Manzo, S., Greenwood, P.** An Impedance Model Based on A Transmission Line Circuit and A Frequency Dispersion Warburg Component for the Study of EIS in Li-ion batteries *Journal of Electroanalytical Chemistry* 871 2020: pp. 114305. http://dx.doi.org/10.1016/j.jelechem.2020.114305
9. **Mohebbi, H., Mirkazemi, S.M.** Influence of Electric Field Strength on Structure, Microstructure, and Electrical Properties of Flash Sintered 8% mol Yttria-stabilized Zirconia as A Solid Oxide Fuel Cell Electrolyte *Ceramics International* 47 (14) 2021: pp. 20220 – 20229. http://dx.doi.org/10.13336/j.1003-6520.hve.20180529045
10. **Abdullah, A.M., Aziz, S.B., Saeed, S.R.** Structural and

Electrical Properties of Polyvinyl Alcohol (PVA): Methyl Cellulose (MC) Based Solid Polymer Blend Electrolytes Inserted with Sodium Iodide (NaI) salt *Arabian Journal of Chemistry* 14 (11) 2021: pp. 103388. http://dx.doi.org/10.1007/s10854-007-9342-1

11. **Scisco, G.P., Orazem, M.E., Ziegler, K.J., Jonesa K. S.** Resistivity of Mesopore-Confined Ionic Liquid Determined by Electrochemical Impedance Spectroscopy *Electrochimica Acta* 378 2021: pp. 138112. http://dx.doi.org/10.1149/MA2020-02453754mtgabs
12. **Brevnov, D.A., Rama Rao, G.V., López, G.P., Atanassov P.B.** Dynamics and Temperature Dependence of Etching Processes of Porous and Barrier Aluminum Oxide Layers *Electrochimica Acta* 49 (15) 2004: pp. 2487 – 2494. http://dx.doi.org/10.1016/j.electacta.2004.02.003
13. **Bendova, M., Pytlicek, Z., Prasek, J.** The Growth and Unique Electronic Properties of the Porous-Alumina-Assisted Hafnium-Oxide Nanostructured Films *Electrochimica Acta* 327 2019: pp. 135029. http://dx.doi.org/10.1016/j.electacta.2019.135029
14. **Starykevich, M., Salak, A.N., Ivanou, D.K., Lisenkov A.D.** Electrochemical Deposition of Zinc from Deep Eutectic Solvent on Barrier Alumina Layers *Electrochimica Acta* 170 2015: pp. 284 – 291. http://dx.doi.org/10.1016/j.electacta.2015.04.150
15. **Dhoke, S.K., Khanna, A.S.** Electrochemical Impedance Spectroscopy (EIS) Study of Nano-Alumina Modified Alkyd Based Waterborne Coatings *Progress in Organic Coatings* 74 (1) 2012: pp. 92 – 99. http://dx.doi.org/10.1016/j.porgcoat.2011.11.020
16. **Jagminas, A., Kurtinaitienė, M., Angelucci, R., Valinčius, G.** Modification of Alumina Barrier-Layer Through Re-Anodization in An Oxalic Acid Solution with Fluoride Additives *Applied Surface Science* 252 (6) 2006: pp. 2360 – 2367. http://dx.doi.org/10.1016/j.apsusc.2005.04.007
17. **Moutarlier, V., Gigandet, M.P., Normand, B., Pagetti J.** EIS Characterisation of Anodic Films Formed on 2024 Aluminium Alloy, In Sulphuric Acid Containing Molybdate or Permanganate Species *Corrosion Science* 47 (4) 2005: pp. 937 – 951. http://dx.doi.org/10.1016/j.corsci.2004.06.019
18. **Ono, S., Masuko, N.** Dissolution Behavior of the Barrier Layer of Porous Anodic Films Formed on Aluminum Studied by Pore-Filling Technique *Journal of Japan Institute of Light Metals* 43 (9) 1993: pp. 447 – 452. http://dx.doi.org/10.1016/S0010-938X(70)80055-5
19. **O'Sullivan, J.P., Wood, G.C.** The Morphology and Mechanism of Formation of Porous Anodic Films on Aluminum *Proceedings of the Royal Society of London Series A* 317 (1531) 1970: pp. 511 – 543. http://dx.doi.org/10.1098/rspa.1970.0129
20. **Thompson, G.E., Xu, Y., Skeldon, P., Shimizu K., Han, S.H., Wood, G.C.** Anodic Oxidation of Aluminium *Philosophical Magazine* 55 (6) 1987: pp. 651 – 667. http://dx.doi.org/10.1080/13642818708218371